CHAPTER III
RESULTS AND DISCUSSION

3.1 Preparation and Characterization of Magnesium Aluminate Spinel by the OOPS Process

The oxide one pot synthesis (OOPS) process is a very simple and low cost of synthesizing rheologically useful precursors to multicomponent oxides. The spinel precursor has been synthesized in up to kilogram quantities within 6-8 h (Tayaniphan, 1995 and Waldner et al, 1996).

Aluminium hydroxide hydrate, [$Al(OH)_3.xH_2O$] and magnesium oxide (MgO) were calcined in the TGA to obtain the exact percentage of Al_2O_3 and MgO before performing the experiments. The ceramic yields for Al_2O_3 and MgO were 62.7% and 95%, respectively. Both values were used throughout the experiments.

The reaction of $Al(OH)_3$, MgO and TEA was completed after 7 h of distillation, and ethylene glycol solvent was removed by vacuum evaporation (10^{-2} torr) at 100°C for 6 h. The yellow colored precursor was very viscous and became a rigid solid at room temperature. The solid product was divided into several parts to determine its solubility and stability in methanol, dichloromethane, chloroform, acetone, ethanol, butanol, isobutanol, and isopropanol. It was shown that the product was not easy to precipitate in 2-5% dried MeOH in dried CH_3CN (Tayaniphan et al, 1995). The product also contains excess TEA which is added to ensure that the reaction goes to completion. The excess TEA is hard to remove by vacuum distillation because of its high boiling point, ~200°C at 5 mm Hg. However, it can be burned out

during precursor pyrolysis. The presence of TEA was confirmed by TGA which showed a lower ceramic yield (29.4 wt.%) than that calculated from theory (32.8 wt.%), as shown in Figure 3.1.

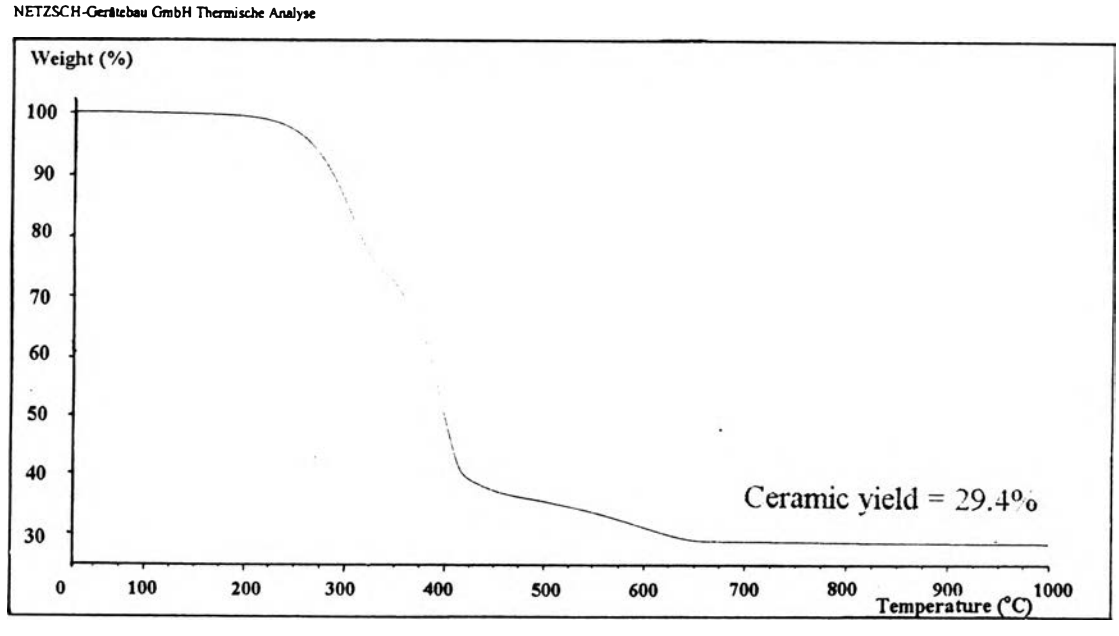

Figure 3.1 TGA of spinel precursor obtained from the OOPS process under synthetic air.

There are three regions of mass loss in the TGA. The first mass loss corresponds to organic ligand decomposition in the range of 220° to 340°C, generating a char as product. The second mass loss is oxidative decomposition of carbon residue (char) at 340° to 600°C. The final mass loss between 600° and 900°C results from decomposition of traces of $MgCO_3$ which forms during organic ligand decomposition. Furthermore, the formation of $MgCO_3$ was confirmed using published literature (Sadtler Research Laboratories, 1965) and previous work (Tayaniphan et al, 1995 and Waldner et al, 1996). The results are indicated by low-intensity and broad peaks at 1640 and 1390 cm^{-1} in

infrared spectra. The intensity of both peaks decreases with increasing pyrolysis temperature, as the carbonate decomposed by losing CO_2.

The mass spectrometry was used to confirm the chemical composition of the double alkoxide product. The parent peak of precursor is the protonated parent ion, observed at m/z 518 (100% intensity). This agrees with data obtained by Waldner et al (1996) and Tayaniphan (1995), see Figure 3.2.

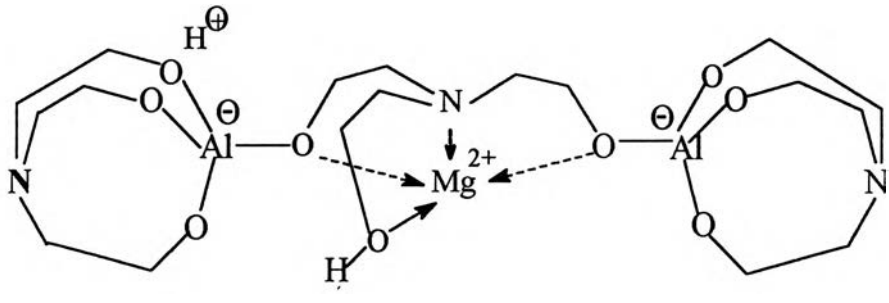

Figure 3.2 Spinel precursor (m/z = 518, 100% intensity).

The structure of the spinel precursor is proposed to be a trimetallic species, consisting of one TEA group per metal center. It was assumed that the Mg^{2+} is actually enfolded by the third TEA, in terms of charge separation. However, there is not an evidence indicating that the bridging TEA actually enfolds the Mg atom. This structure reasonably minimizes the charge separation and appears to be the most stable environment for the dipositive cation. Thus, the electrostatic interactions are diminished. A disordered and amorphous precursor forms on heating at ~100°C that shows the viscoelastic behaviour. Due to the ion mobility (diffusion), the weaker electrostatic interaction may be induced to occur by heating.

The ^{1}H-NMR of the spinel precursor, is presented in Table 3.1 and shows the peak positions for methylene groups adjacent to oxygen and nitrogen atoms, occurring at chemical shifts of 3.73 ppm (triplet) and 2.72 ppm (triplet),

respectively. The integration ratio of CH_2-O:CH_2-N was 1:1. The peak positions for these methylene groups were not identical in chemical shifts, indicating that the methylene groups adjacent to oxygen and nitrogen atoms have different environments and are affected from the different neighbour groups.

Table 3.1 ^{1}H-NMR peak positions and assignments for spinel precursor

Chemical Shift (ppm)	Tentative Assignments
2.67 (t)	N(**CH_2**$CH_2OH)_3$, free TEA
3.65 (t)	N(CH_2**CH_2**$OH)_3$, free TEA
4.5 (br)	OH either from free of Mg^{2+} coordinated TEA
2.72 (t)	CH_2 adjacent to N
3.73 (t)	CH_2 adjacent to O

^{13}C-NMR of spinel precursor (see Table 3.2) shows the peak positions corresponding to the carbon positions in the spinel precursor and for some free TEA. It is not possible to distinguish between free TEA and bridging groups. Furthermore, TEA is difficult to remove from the reaction because of its high boiling point, the free TEA was thus retained in the precursor. The excess TEA decreases the ceramic yield as seen in the TGA.

Table 3.2 ^{13}C-NMR peak positions and assignments for spinel precursor

Chemical Shift (ppm)	Tentative Assignments
52.7	$N(\mathbf{CH_2}CH_2OH)_3$, free TEA
52.8	$N(\mathbf{CH_2}CH_2O)Al$ (also free TEA)
56.7	bridging, $N(\mathbf{CH_2}CH_2O)$
56.3	$N(CH_2\mathbf{CH_2}O)Al$
59.5	bridging, $N(CH_2\mathbf{CH_2}O)$
63.6	$N(CH_2\mathbf{CH_2}OH)_3$, free TEA

The spinel obtained after pyrolysis of the precursor at 1100°C for 2 h was a white powder. Since the precursor is highly viscous, this viscosity limits escape of the decomposition products, namely, CO, CO_2, H_2O, and volatile hydrocarbon products, produced during precursor decomposition. Thus, a gas-filled and foam-like structure forms which is retained as a porous structure during pyrolysis.

X-ray diffraction analysis was conducted on spinel samples heated to 1100°C for 2 h under air. The relative intensities of the XRD patterns are shown in Figure 3.3.

All the peak positions were identified by comparing with JCPDS file No. 21-1152. The major peaks for spinel were the 311 hkl reflection (d = 0.244 nm, I = 100%) and 400 hkl reflection (d = 0.202 nm, I = 56%). The method of Pasquier et al (1991) was used to follow the phase evolution as a function of pyrolysis temperature by comparing the relative intensity ratio of the 400 and 311 peaks. A value equals to 0.6 was found for a commercial high purity spinel (Baikowski International). The relative intensity ratio of the 400 and 311 peaks of product obtained after pyrolysis, was 0.56, as the material transforms to pure spinel. This value agrees well with previous works

(Waldner et al, 1996 and Tayaniphan et al, 1995). Additionally, the XRD pattern exhibited sharp scattering peaks of typical crystalline materials (West, 1989).

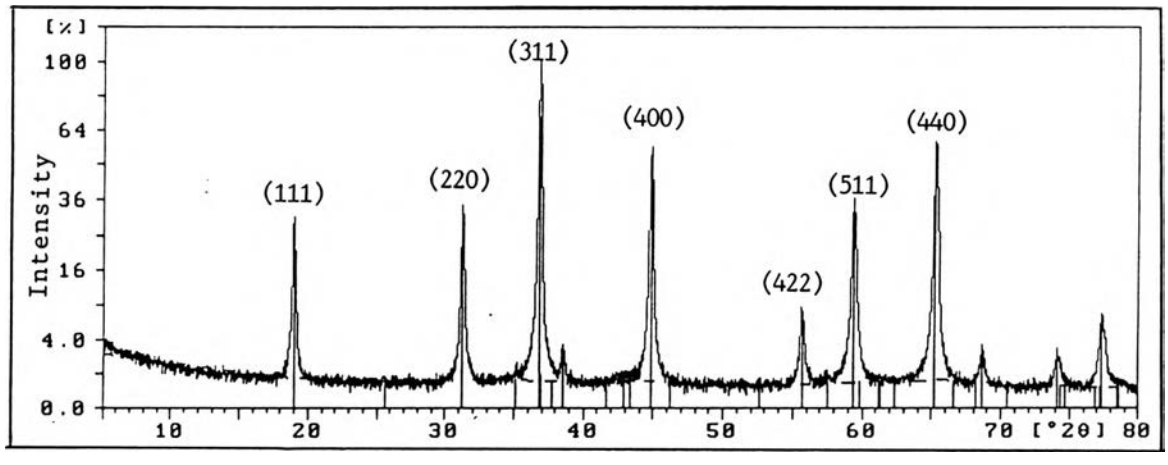

Figure 3.3 XRD pattern of spinel powder obtained after pyrolysis of the precursor at 1100°C for 2 h in air.

The specific surface area of the 1100°C spinel powder was measured by BET analysis to be 11.2 m^2/g. The crystallite size and grain sizes were determined by SEM compare favorably with the average particle diameters derived from the BET surface area and the XRD data. The equivalent spherical diameter predicted from the surface area was 150 nm. The average crystalline sizes of spinel powder determined using the Debye-Scherrer equation from a line broadening technique which measures the full width at half-intensity of the largest intensity reflection of XRD pattern, was 390 nm.

The surface area measurements were confirmed by SEM observations, as shown in the electron micrograph, Figure 3.4. The powder was irregularly shaped with more perfect grain and blocky particles possibly due to excessive necking between grains occurred during pyrolyzing the precursor. This

occurrence led to the larger grain size and less surface area. The sizes range from submicron to greater than 50 μm.

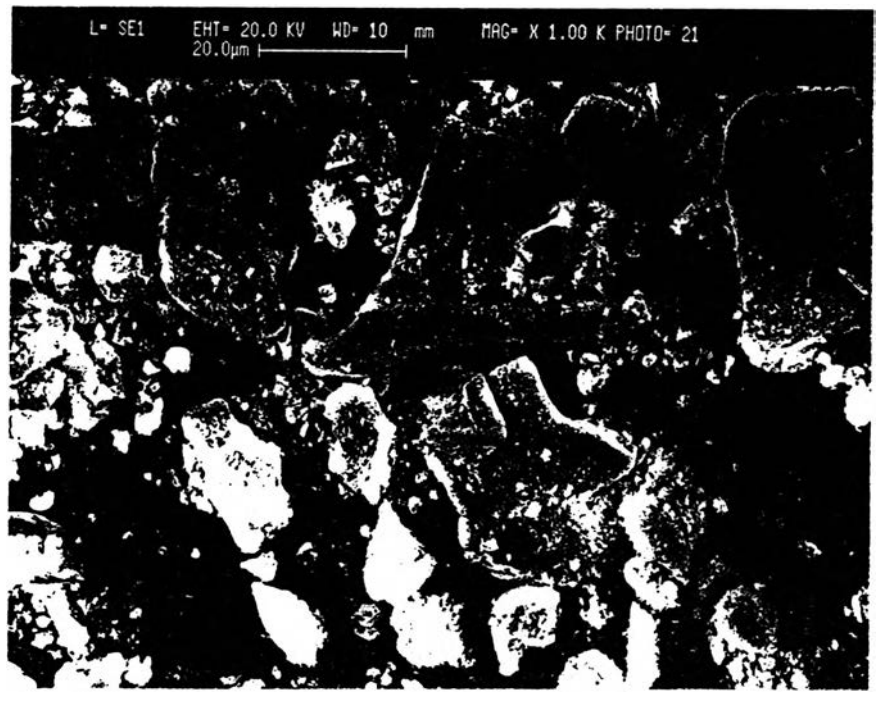

Figure 3.4 SEM of spinel powder obtained after pyrolysis of the precursor at 1100°C for 2 h in air.

3.2 Preliminary Studies of Magnesium Aluminate Pellets as Humidity Sensors

Initial studies on the use of spinel as a humidity sensing element focused on the pellet form. It was found that the as-fired spinel powder was difficult to compress and the pellet broke after released from the mold due to the strength, compactness and irregularity of the powder. Therefore, it is essential to reduce the agglomeration of the spinel powder by milling with ball-milling or grinding in a mortar and pestle. Before compressing the spinel powder, sieving at 200 mesh was carried out to remove larger particles.

The powder used for preparing the pellets was obtained by decomposing the precursor from the OOPS process at 1100°C for 2 h and subsequently ball-milling and sieving. After the pellets were sintered at 1100°C for 2 h and 1300 °C for 8 h under air atmosphere. Their microstructures were studied by using SEM and mercury porosimetry measurements. The micrographs are shown in Figures 3.5 and 3.6 for both pellets.

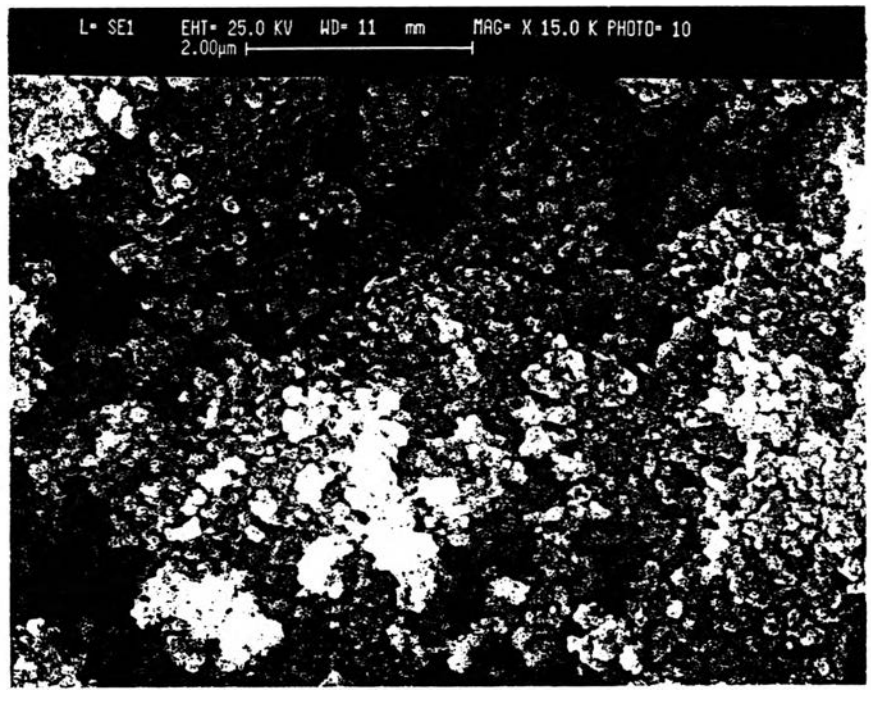

Figure 3.5 SEM of pellet sintered at 1100°C for 2 h in air.

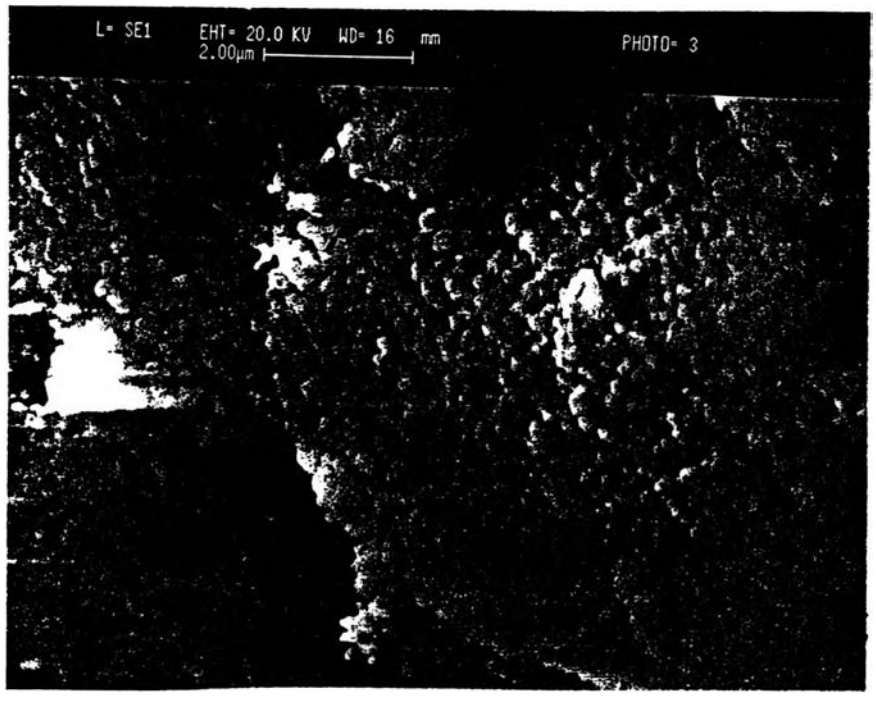

Figure 3.6 SEM of pellet sintered at 1300°C for 8 h in air.

The mercury porosimetry is suitable for characterization of the pore size distribution in the compact. Since mercury does not easily wet most materials or enter the pores, gradual increase in pressure is applied to force the mercury into the pores, and the volume intruded at each pressure is measured. The pressure required is a function of the pore size distribution. This measurement was used to confirm the SEM results, as well. The results indicate that variations in sintering temperatures and times affects not only on the total open porosity but also the pore size distribution. Both pellets exhibited the bimodal pore distributions. The pellet sintered at 1300°C for 8 h has a 29.1% total porosity, with 21.1% of the pores smaller than 100 nm, while the remaining pores were concentrated in the range 100-1000 nm. Pellets sintered at 1100°C for 2 h have the total porosity of 40%, with 60.5% of the pores being <100 nm and 39.5% of pores in the 100-1000 nm range. Longer sintering time also affected microstructures as the particles had more time sinter.

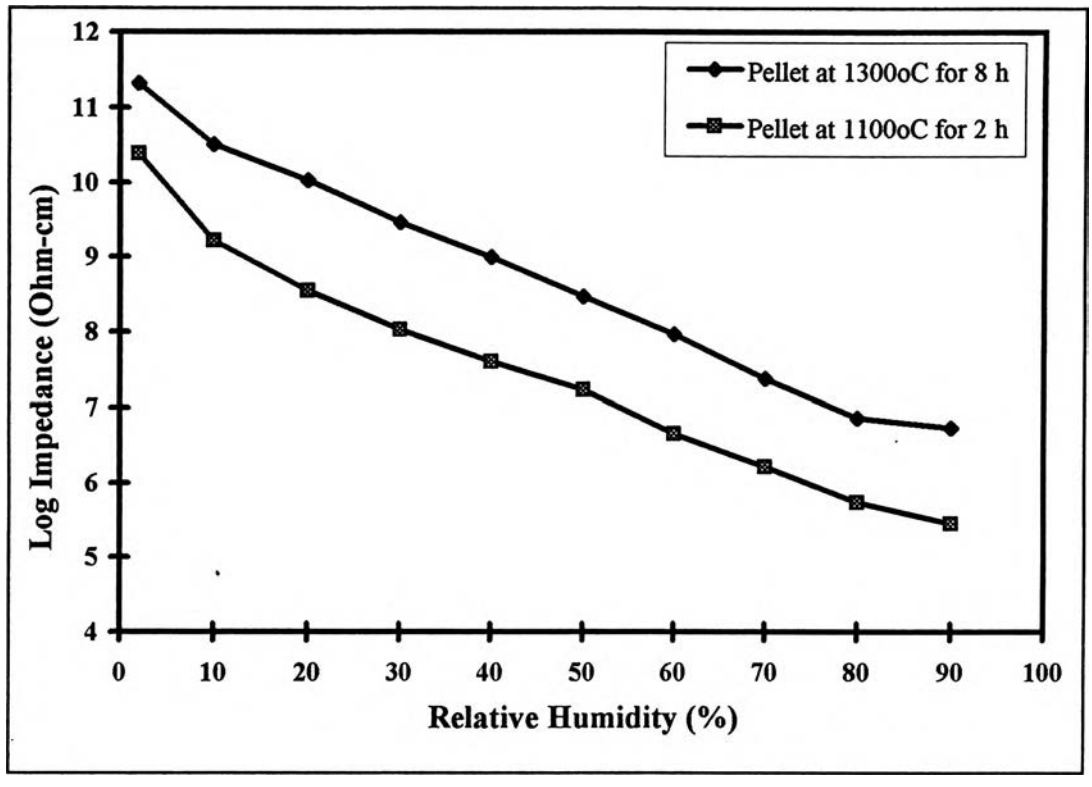

Figure 3.7 Relationship between log impedance of $MgAl_2O_4$ pellets sintered at 1100°C for 2 h and at 1300°C for 8 h in air, and a relative humidities of 2-90%.

The observed impedance-humidity characteristics of $MgAl_2O_4$ pellets sintered at 1100°C for 2 h and at 1300°C for 8 h under air atmosphere, at relative humidity (RH) between 2-90% at 40°C are shown in Figure 3.7.

The conduction mechanism for sintered $MgAl_2O_4$ pellets is ionic and conductivity increases with increasing chemisorption, physisorption, and/or capillary condensation of water within the pore structure (Gusmano et al, 1993). The resistance decreases with increasing relative humidity, showing that the conduction occurs mainly at the grain surface by means of ionic carriers and is governed by total water molecules content.

When dry samples are first exposed to moist air, a monolayer of vapor molecules chemisorb on the oxide surface and dissociate to form two hydroxyls. The hydroxyl groups adsorbed on a surface of metal ion dissociate to protons and adjacent oxygen ions (Nitta et al, 1980; and Gusmano et al, 1993). The hydroxyl groups dissociate and provide mobile protons (H^+). At this stage, the charge carriers are proton, therefore, electrical conduction occurs by proton hopping between adjacent hydroxyl groups. The high activation energy required to dissociate hydroxyl groups is reflected in the low conductivity and/or high resistivity in the first layer of water molecules at low relative humidity.

By increasing the humidity level, subsequent layers of water molecules are physisorbed on the first hydroxyl layer. Each water molecule of the first layer of physical adsorption is bonded to two hydroxyls (Nitta et al,1980 and Gusmano et al, 1993) and cannot move or rotate freely upon application of an external electric field (Yamazoe et al, 1986). In the successive physisorbed layers, water molecules are singly hydrogen bonded to the water molecules in the layer below and more free to rotate which is important for Grotthuss-type transport of proton (Yamazoe et al, 1986). Higher carrier concentration is found when more than one layer of physisorbed water molecules is present on the surface.

The easy dissociation of physisorbed water, due to the high electrostatic fields in the chemisorbed layer, produces H_3O^+ ions which cause electrical conduction by charge transport via a Grotthuss chain reaction, the H_3O^+ will be hydrated in the presence of enough adsorbed water, as shown in the equation 3.1 and Figure 3.8.

$$H_2O + H_3O^+ \rightleftharpoons H_3O^+ + H_2O \qquad (3.1)$$

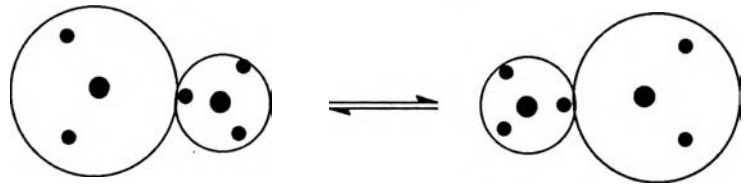

Figure 3.8 Grotthuss chain reaction (Sun et al, 1989).

Thus, the charge transport mechanism depends on the surface coverage of the physisorbed water molecules. It is due to H_3O^+ diffusion on the hydroxyl groups and proton transfer between adjacent water molecules in clusters when the surface coverage is not complete, whereas it is governed by the proton hopping from one water molecule to the other when the water layer is continuous. The activation energy required to dissociate water is lower than that needed to dissociate hydroxyl groups, resulting in higher conductivity or lower resistivity at the high relative humidity. A higher carrier concentration is therefore found when more adsorbed water layers are present on the pellet surface. This ionic mechanism was also found by other authors for other types of ceramics (Nitta et al, 1980; Sadaoka et al, 1987; Yeh et al, 1990; and Gusmano et al, 1993).

Additionally, the humidity-sensitive electrical response of the pellets was also found to be related to their microstructure. At different relative humidity values, the presence of pores is not only effective in increasing the specific surface area, but also in permitting capillary condensation of water within the pores, which results in electrolytic conduction in addition to protonic conduction (Gusmano et al,1993). Based on the Kelvin equation, theoretical calculations showed that at 40°C, water condensation takes place in capillary pores with radii <0.2 nm at near 0% relative humidity, and with radii lower than 4-6 nm at 80% relative humidity (Gusmano et al, 1993). Thus, the

electrical behaviour of pellets is influenced both by total porosity and pore size distribution. The lower resistance values are found to be related to larger total open porosity, and to the presence of a greater number of pores larger than 100 nm. Pellets sintered at 1100°C for 2 h had the lowest impedance, as expected based on the higher open porosity. The decrease in resistance at low relative humidity is also related to the presence of pores small enough to permit capillary condensation. In fact, from the results obtained from SEM and porosity measurement for both pellets, they did not have pores with radii <0.2 nm thus at nearly 0% RH, the impedance of pellet sintered at 1100°C for 2 h was lower than that sintered at 1300°C for 8 h due to the effect of the total porosity. The pellet sintered at 1300°C for 8 h has pore radii in the range 1-10 nm around 0.28% VS. 3.47% for that sintered at 1100°C for 2 h. Thus, the pellet sintered at 1300°C for 8 h has much higher impedance at high relative humidity level than another one.

To characterize the properties of electroceramics related to there microstructure, measurement techniques are required that can probe or distinguish between the electrical behaviour of the differents regions of a ceramic microstructure. One of the most useful techniques, ac impedance measurements made over a wide range of frequencies, was used. According to electrical relaxation times or time constants, different regions of a material can be characterized and distinguished easily by this technique. The impedance of samples were measured over a wide range of frequency, typically 10^{-2}-10^{9} Hz, to determine both resistive and reactive (capacitive/inductive) components. For our samples, the data obtained form a semicircular plot of imaginary, Z" against real, Z' impedances. This means that the equivalent electrical circuit can be described by a resistor (R) and a capacitor (C) in parallel. Thus, R values are obtained from the intercepts on the Z' axis and C values are evaluated at the maximum of each semicircle. From complex impedance plane plots provides values of component resistances and capacitances and also

indicates whether the overall resistance of a material is dominated by bulk or grain boundary components. The impedance spectra of electroceramics can also show the presence of distinct features attributable to intergrain, or bulk and intergrain, or grain boundary regions.

The specific assignments are based on the magnitudes of capacitances (Irvine et al, 1990 and Gusmano et al, 1993). The capacitances obtained for both pellets were around 10^{-11} F at each relative humidity level associated with the resistance. They showed the presence of two distinct features of humidity/grain interaction and grain/electrode interaction (Irvine et al, 1990, Gusmano et al, 1993 and Traversa, 1995).

When pellets were exposed to a humid environment for a long time, an increase in resistance was observed. This is called the drift effect and is caused by gradual formation of stable chemisorbed OH^- ions on the oxide surface following prolonged exposure in a humid environment. Due to the ionic type humidity sensing mechanism, proton hopping is adversely affected by the presence of surface hydroxyl ions instead of water molecules, thereby decreasing surface conductivity. In addition, another problem affecting sample response is deterioration due to adhesion of dust, dirt, oil, or other organic vapors (Nitta et al, 1980 and Gusmano et al, 1993). The humidity sensitivity degrades remarkably even for short exposure times. However, heat cleaning at >400°C for 5 min. recovers spinel performance and is easy and effective. The results indicate that the pellets exhibit a good humidity sensitivity, good linearity and reproducibility in relative humidity range from 2 - 90%. The use of pellets sintered at lower temperature (1100°C) is more effective because it shows lower impedances over the entire RH range and same sensitivity.

3.3 Preparation of Spinel Directly from Aluminium Hydroxide and Magnesium Hydroxide

The solid-state reactions occur at the surfaces of solids where they touch each other due to lattice imperfections or the defects. One of the factors that influences the rate of reaction between solids is their surface areas. The mixing of both reactants by ball-milling was used before sintering the mixed powder to obtain the maximized surface areas, as well as to bring fresh surfaces into contact, and hence a better reaction rate.

The spinel powder prepared directly from aluminium hydroxide and magnesium oxide has been studied for a long time that is shown by Wagner reaction mechanism (Kingery et al, 1975 and West, 1989). Initially, there is only a single phase boundary between the reactants. After the nucleation of the product phase, this boundary is replaced by two different phase boundaries. At a later stage reaction occurs only by transport of the reactants through the product phase. Then, the mechanism at this stage involves the counter diffusion of Mg^{2+} ions, Al^{3+} ions, or O^{2-} ions through the product layer followed by further reaction at two reactant-product interfaces, MgO-$MgAl_2O_4$ or $MgAl_2O_4$-Al_2O_3. However, two possible mechanisms may occur wherein oxygen is transported through the gas phase by a loss and it was subsequent taken up due to oxidation-reduction mechanisms at the phase boundaries on the respective sides of the interface (Kingery et al, 1975 and West, 1989). The mechanism of a solid-state reaction is discussed with the aid of a schematic diffusion-couple arrangement, as shown in Figure 3.9.

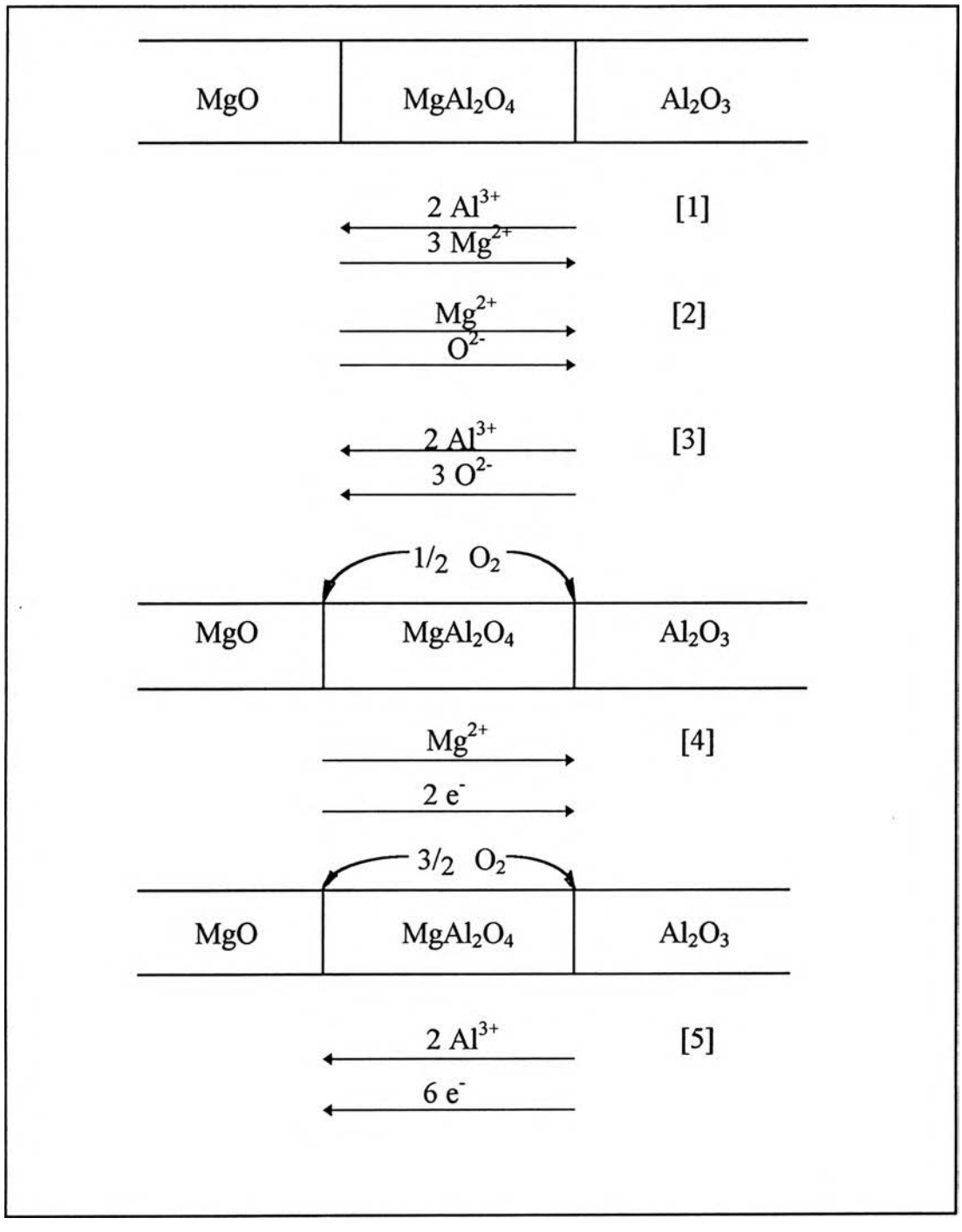

Figure 3.9 Schematic representation of several mechanisms that may possibly occur in the spinel preparation by solid-state reaction (Kingery et al, 1975 and West, 1989).

The possible reaction paths undergone at two interfaces may be described ideally as follows:

(1) Both cations, namely Mg^{2+} ion and Al^{3+} ion diffuse to contact surfaces of the reacting components. The ions diffusion also means the simultaneous transport of the electrical charges. Then, the net electrical charge flowing across the reaction layer must be zero and in order to maintain charge balance, for every three Mg^{2+} ions which diffuse to the right-hand interface, two Al^{3+} ions must diffuse to the left-hand interface as shown in Figure 3.9.

(a) Reaction occurs at $MgO/MgAl_2O_4$ interface.

$$2\ Al^{3+} - 3\ Mg^{2+} + 4\ MgO \longrightarrow MgAl_2O_4$$

(b) Reaction occurs at $MgAl_2O_4/Al_2O_3$ interface.

$$3\ Mg^{2+} - 2\ Al^{3+} + 4\ Al_2O_3 \longrightarrow 3\ MgAl_2O_4$$

(c) Overall reaction

$$4\ MgO + 4\ Al_2O_3 \longrightarrow 4\ MgAl_2O_4$$

It can be seen that reaction (b) gives three times as much spinel product as reaction (a) and, hence, the right-hand interface should grow or move at three times the rate of the left-hand interface.

(2) Mg^{2+} ion and O^{2-} ion diffuse and the reaction occurs at $MgAl_2O_4/Al_2O_3$ interface.

$$Mg^{2+} + O^{2-} + Al_2O_3 \longrightarrow MgAl_2O_4$$

(3) Al^{3+} ions and O^{2-} ions diffuse and the reaction occurs at $MgO/MgAl_2O_4$ interface.

$$2\,Al^{3+} + 3\,O^{2-} + MgO \longrightarrow MgAl_2O_4$$

(4) Reaction occurs at $MgAl_2O_4/Al_2O_3$ interface as the oxygen gas phase is transported with Mg^{2+} ion and electron is transported through $MgAl_2O_4$.

$$Mg^{2+} + 2\,e^- + 1/2\,O_2 + Al_2O_3 \longrightarrow MgAl_2O_4$$

(5) Reaction occurs at $MgO/MgAl_2O_4$ interface as the oxygen gas phase is transported with Al^{3+} ions and electron transported through $MgAl_2O_4$.

$$2\,Al^{3+} + 6\,e^- + 3/2\,O_2 + MgO \longrightarrow MgAl_2O_4$$

The XRD pattern of the product obtained on reacting $Al(OH)_3$ and MgO at 1100°C for 15 h in air, is shown in Figure 3.10. All peak positions are identified by comparing with standard JCPDS files No.21-1152 for spinel and No.04-0829 for MgO. One of major peaks of MgO (2θ = 43, d = 0.211 nm, I = 36.5 %) gave high intensity as compared to the major peak of spinel (hkl = 311, d = 0.244 nm, I = 100%), indicating that the reaction between aluminium hydroxide, [$Al(OH)_3$], and magnesium oxide, (MgO), was incomplete due to the presence of unreacted MgO and presumable $Al(OH)_3$. Furthermore, this occurrance probably results from a change in the ratio between $Al(OH)_3$ and MgO, or the incorrect stoichiometries resulting from mechanical loss of sample during sample preparation or solid-state reaction.

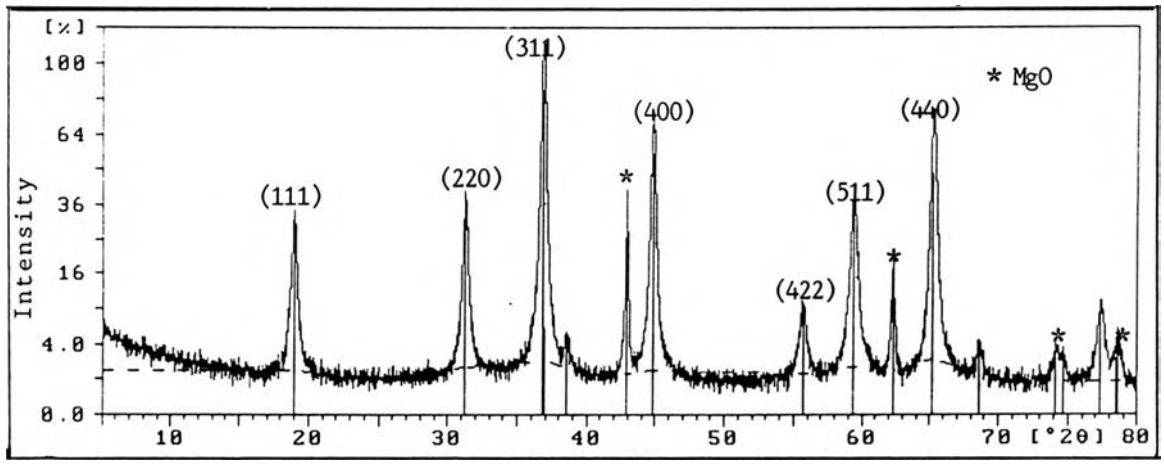

Figure 3.10 XRD pattern of spinel powder prepared by solid-state reaction at 1100°C for 15 h in air.

The major peaks for spinel obtained from the solid-state reaction at 1100 °C for 15 h were the 311 hkl reflection (d = 0.244 nm, I = 100%) and 400 hkl reflection (d = 0.202 nm, I = 73.5 %). Thus, the relative intensity ratio of the 400 and 311 peaks was 0.735, as the product had not transformed to pure spinel (Tayaniphan et al,1995).

The BET surface area of the product obtained was 28 m^2/g and the average particle diameters calculated from BET surface area and the Debye-Scherrer equation were 60 nm and 270 nm, respectively. The results indicated that the product obtained had high surface area because the product was composed of large amount of the reactant, MgO, and/or it did not transform to pure spinel as suggested by the relative intensity ratio of the 311 and 400 peaks.

The first step in the reaction was the formation of $MgAl_2O_4$ nuclei at the reactant interfaces. This nucleation is rather difficult due to the fact that the structures between reactants [$Al(OH)_3$ or Al_2O_3 and MgO] and product ($MgAl_2O_4$) were different, and structural reorganization involving in product formation was quite large. Therefore, chemical bonds breaking and reforming, occurred (Kingery et al, 1975; West, 1989; and Koller, 1994).

The chemical reactions of substances in the solid state are assumed to occur by ions diffusing through crystals (see Figure 3.9). Diffusion is directly related to the motion of vacancies that replace the moving ions. The jump of ions from one nodal position to the next is dependent on a certain amount of energy being available to overcome the energy barrier, the activation energy. The new phase that forms (the nucleation step) will not occur without this activation energy. Increases in temperature above 1100°C are needed to increase the energy of ions and overcome the activation energy (West, 1989 and Koller, 1994).

Although the ions have sufficient thermal energy at higher temperatures to diffuse through the crystals, the rate of reaction is limited by the thickness of new phase layer. Further reaction increases the spinel content increasing the diffusion distances slowing the entire process. Consequently, the course of the reaction depends mostly on the rate of reactant transport to the reaction site, i.e. not only the initial components, but also the reaction intermediates (Kingery et al, 1975; Anthony, 1989; and Koller, 1994).

Additionally, the solid-state reactions need more than 15 h heating to completion the reactions and obtain the highest conversion to product. Consequently, the average grain size increases because the rate of spinel formation is a function of heating time (Kingery et al, 1975 and West, 1989). Another spinel was therefore prepared by sintering in air at the same sintered temperature of 1100°C for 20 h and the product was investigated by XRD, BET and SEM to confirm this assumption.

From the XRD pattern of the product obtained on reacting $Al(OH)_3$ and MgO at 1100°C for 20 h in air, Figure 3.11, all the peak positions were identified by comparing with standard JCPDS files No.21-1152 for spinel and No.04-0829 for MgO. One of the major peaks of MgO ($2\theta = 43$, $d = 0.211$ nm, $I = 19.6$ %) showed moderate intensity as compared to the major peak of spinel (hkl = 311, d = 0.244 nm, I = 100%), indicating the incomplete reaction.

However, the results showed that the XRD intensity of the MgO peak decreases with increasing reaction time.

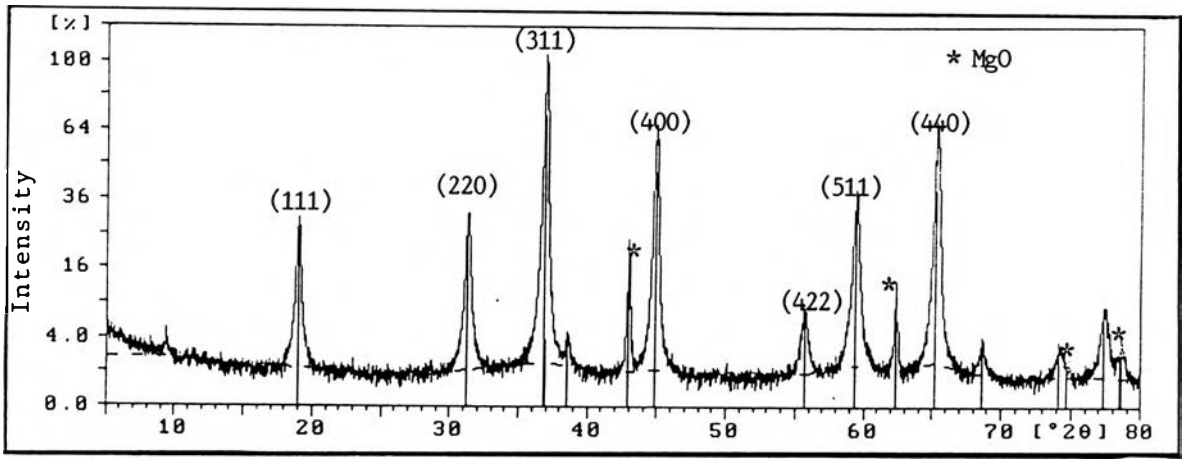

Figure 3.11 XRD pattern of spinel powder prepared by solid-state reaction at 1100°C for 20 h in air.

Furthermore, the relative intensity ratio of the 400 and 311 peaks, is 0.622, as the product transforms to pure spinel (Tayaniphan et al,1995). The BET surface area obtained, 14 m^2/g, is lower than the 15 h product. The average particle diameter calculated from the BET surface area and derived from the Debye-Scherrer equation were 120 nm and 340 nm, respectively. The XRD, BET, and SEM (see Figure 3.12 and 3.13) results indicate that the grain size of product heated for 20 h is larger than for 15 h.

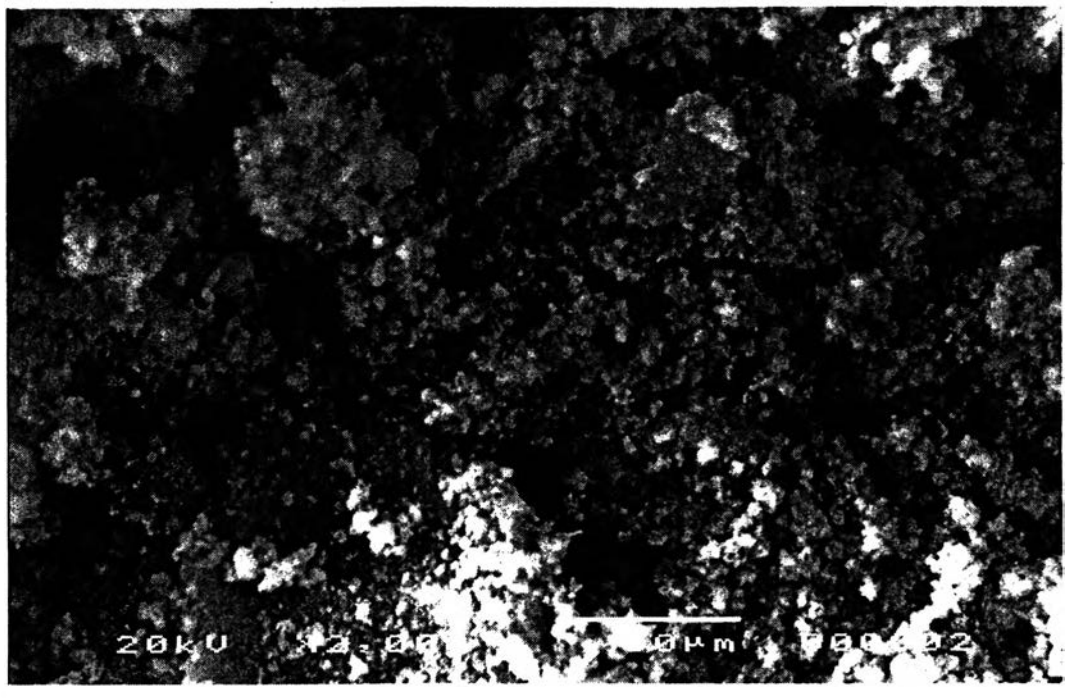

Figure 3.12 SEM of spinel product obtained by solid-state reaction at 1100^{O}C for 15 h in air.

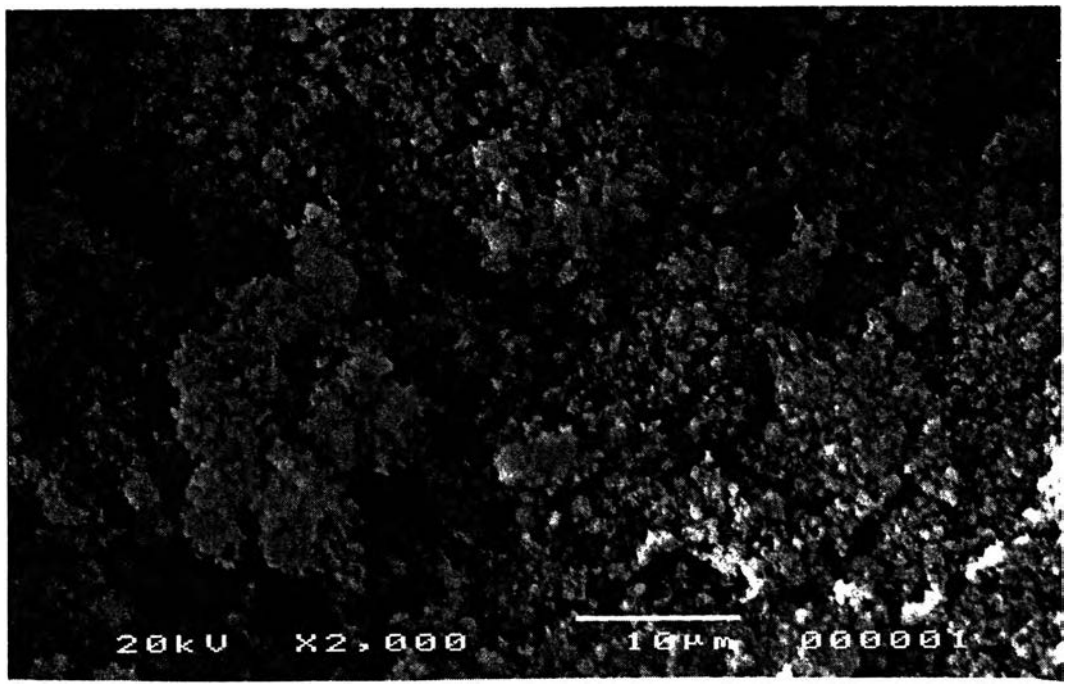

Figure 3.13 SEM of spinel product obtained by solid-state reaction at 1100^{O}C for 20 h in air.

3.4 Preparation of spinel from Alumatrane and $Mg(OMe)_2$

Based on previous work, tris(glycolato)silicate complexes can be prepared by the oxide one pot synthesis (OOPS) process and an alternate synthesis. The alternate synthesis gives improved yields, compared to MgO used in the OOPS process, when the starting materials are SiO_2 to $Si(OEt)_4$ and MgO to $Mg(OMe)_2$. Thus, an alternate synthesis for spinel precursor was developed that used $Mg(OMe)_2$ and alumatrane to be reactants instead of MgO and $Al(OH)_3$.

$Al(OH)_3$, triethanolamine (TEA) and ethylene glycol (EG) were first mixed homogeneously at room temperature to obtain a milky solution. After heating to 200°C, the solution started to turn clear. A clear, yellow solution was obtained after the reaction was completed in 6 h (100% conversion assumed).

Mass spectral analysis of the product before precipitating indicates that it is oligomeric. The base peak is attributed to the dimeric alumatrane complex (m/z = 347, 100% intensity) which appears to be the most stable species as shown in Figure 3.14.

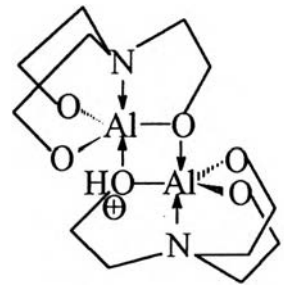

Figure 3.14 Dimeric alumatrane (m/z = 347, 100% intensity).

A reaction of the magnesium powder and dried methanol was carried out, as shown in equation 3.2. The methoxide in methanol acted as a nucleophile to react with magnesium acted as an active metal. The hydronium ion was replaced by the metal to liberate hydrogen gas and form magnesium methoxide (Ozaki, 1988), since polarity of the O-H bond of methanol facilitates the separation of the positive proton while the electronegativity of oxygen readily accommodates the negative charge of electrons (Morrison et al, 1987).

$$Mg\,(s) + 2\,CH_3OH \longrightarrow Mg(OCH_3)_2 + H_2\,(g) \qquad (3.2)$$

When the magnesium powder dissolves completely in methanol, a turbid solution was obtained. The magnesium methoxide [$Mg(OMe)_2$] reacts with ethylene glycol (EG) added into the mixture leading to replacement of methoxide by ethylene glycol, as shown in equations 3.3 and 3.4. This reaction is called alcoholysis reactions (Mehrotra, 1988). The $Mg(eg)_2$ complex obtained was a white gel.

$$Mg(OCH_3)_2 + HOCH_2CH_2OH \longrightarrow Mg(OCH_3)(OCH_2CH_2OH) + CH_3OH \qquad (3.3)$$

$$Mg(OCH_3)_2 + HOCH_2CH_2OH \longrightarrow Mg(OCH_2)_2 + 2\,CH_3OH \qquad (3.4)$$

After adding triethanolamine (TEA) and alumatrane to the magnesium alkoxide mixture, the mixture was then heated to 200°C. The temperature was constant around 110°-125°C since by-products, CH_3OH, water azeotropically distill off. When the temperature increased to 198°-200°C while the $Mg(eg)_2$ gel that formed slowly dissolved. The reaction was complete in 2 h and resulted in a clear, orange colored solution. Ethylene glycol was removed by

vacuum distillation at 10^{-2} torr (100°C/8 h). The clear, brown colored precursor was very viscous and became solidified at room temperature.

The TGA of spinel the precursor was in agreement with that obtained in section 3.1. However, the ceramic yield obtained (28.9 wt.%), as shown in Figure 3.15, was lower than theory (32.8 wt.%) and not different than from the section 3.1 (29.4 wt.%) results. This is because excess TEA has been added to ensure that the reaction goes completion, and again it is difficult to remove TEA from spinel precursor product by vacuum distillation because of its high boiling point.

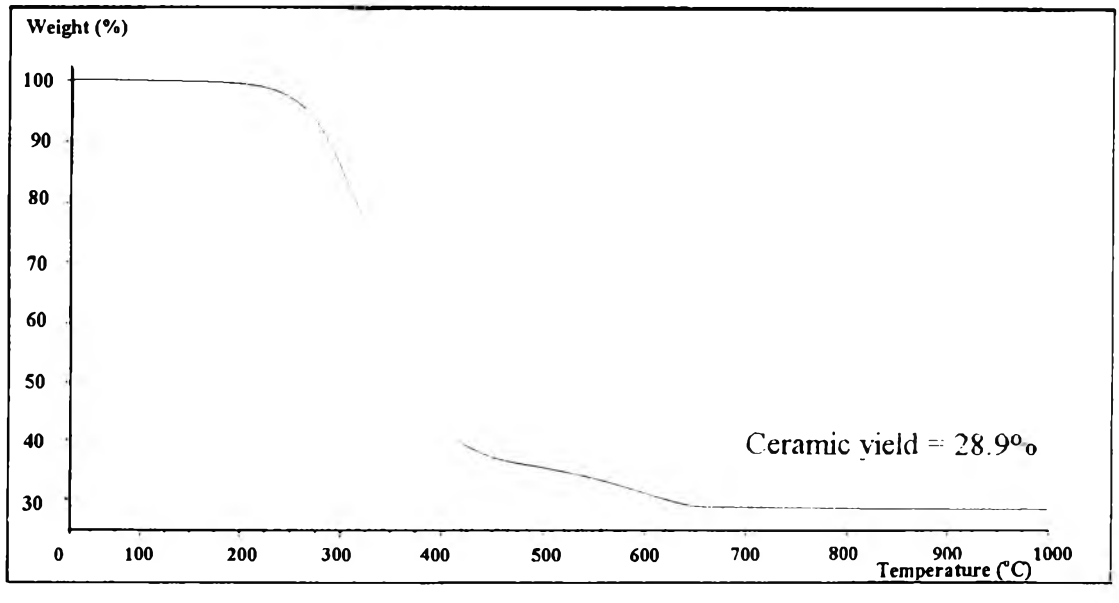

Figure 3.15 TGA of spinel precursor prepared from alumatrane and $Mg(OMe)_2$ in synthetic air.

To confirm the chemical composition of double alkoxide product, the mass spectrometer was used. The parent peak is the protonated ion, observed in the mass fragmentation spectral at m/z = 518 (100% intensity).

The ^{1}H-NMR spectrum of the spinel precursor showed chemical shifts in ppm unit for methylene groups adjacent to nitrogen and oxygen atoms, occurring at 2.75 (triplet) and 3.74 (triplet), respectively. The integration ratio of CH_2-O:CH_2-N was 1:1. The peak positions of both methylene groups did not have the same chemical shift because they were affected by the neighbouring groups which had different electronegativites. Oxygen atom had more electronegativity than nitrogen atom, therefore, the methylene group adjacent to oxygen atom was more deshielded than the methylene group adjacent to nitrogen. The chemical shift of CH_2-O was farther from TMS than that of CH_2-N. Table 3.3 summarizes the ^{1}H-NMR data for the spinel precursor prepared from alumatrane and $Mg(OMe)_2$.

Table 3.3 ^{1}H-NMR peak positions and assignments for spinel precursor prepared from alumatrane and $Mg(OMe)_2$

Chemical Shift (ppm)	Tentative Assignments
2.60 (t)	$N(\mathbf{CH_2}CH_2OH)_3$, free TEA
3.60 (t)	$N(CH_2\mathbf{CH_2}OH)_3$, free TEA
5.3 (br)	OH either from free of Mg^{2+} coordinated TEA
2.75 (t)	CH_2 adjacent to N
3.74 (t)	CH_2 adjacent to O

The precursor was then sintered to obtain spinel, as mentioned in the section 3.1. High viscosity of spinel precursor limited escape of the decomposition products, namely, CO, CO_2, volatile hydrocarbon fragments, and H_2O produced during decomposition of precursor. Thus, a gas-filled foam like structure was formed during pyrolyzing and was retained as a porous structure (Waldner et al, 1996).

X-ray diffraction analysis characterized spinel powder obtained from pyrolyzing the precursor for 2 h under air atmosphere. The standard JCPDS file No. 21-1152 was utilized to identify all peaks of spinel sample and the method of Pasquier et al (1991) was used for the phase evolution of crystalline spinel.

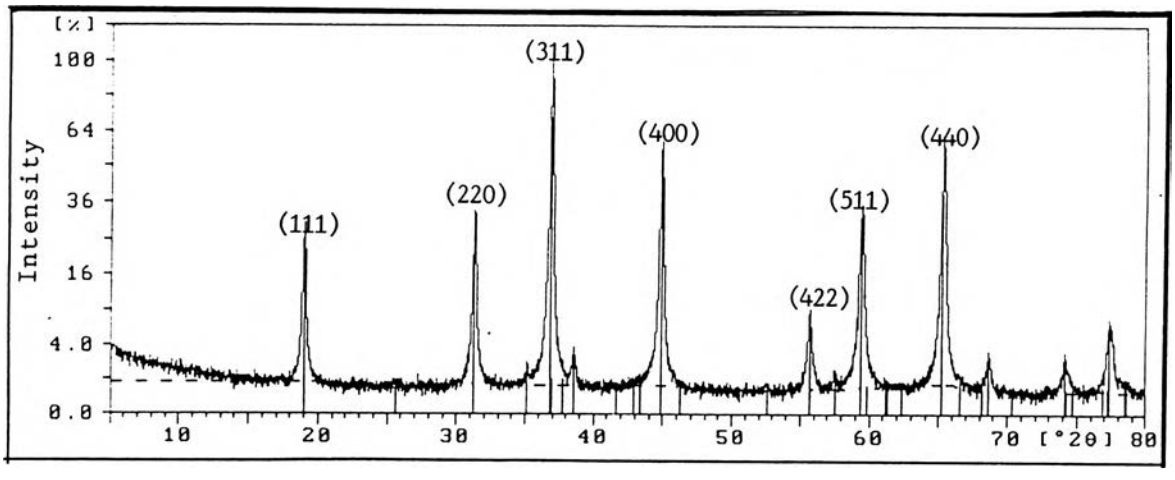

Figure 3.16 XRD pattern of spinel powder prepared by sintering precursor obtained from the reaction of alumatrane and $Mg(OMe)_2$ at 1100°C for 2 h in air.

The major peaks of XRD patterns (Figure 3.16) were the 311 hkl reflection (d = 0.244 nm, I = 100%) and 400 hkl reflection (d = 0.202 nm, I = 56%). The relative intensity ratio of the 400 and 300 peaks, was 0.56 which showed that the product has transformed to the pure spinel, as compared to the value from a commercial high purity spinel (Baskowski International) and agreed with the previous works (Waldner et al, 1996 and Tayaniphan et al, 1995).

The product was then charaterized its microstructure by BET analysis. Its specific surface area was 7 m^2/g. The average spherical diameter predicted from the surface area was 240 nm. The average crystallite size of spinel

powder determined using the Debye-Scherrer equation was 394 nm. SEM measurement confirmed the microstructure of powder obtained after being sintered, as shown in Figure 3.17. The powder was in blocks with more perfect grain size, and was irregularly shaped due to the strong necking of unit particles. Thus, the size of powder was larger than 50 μm.

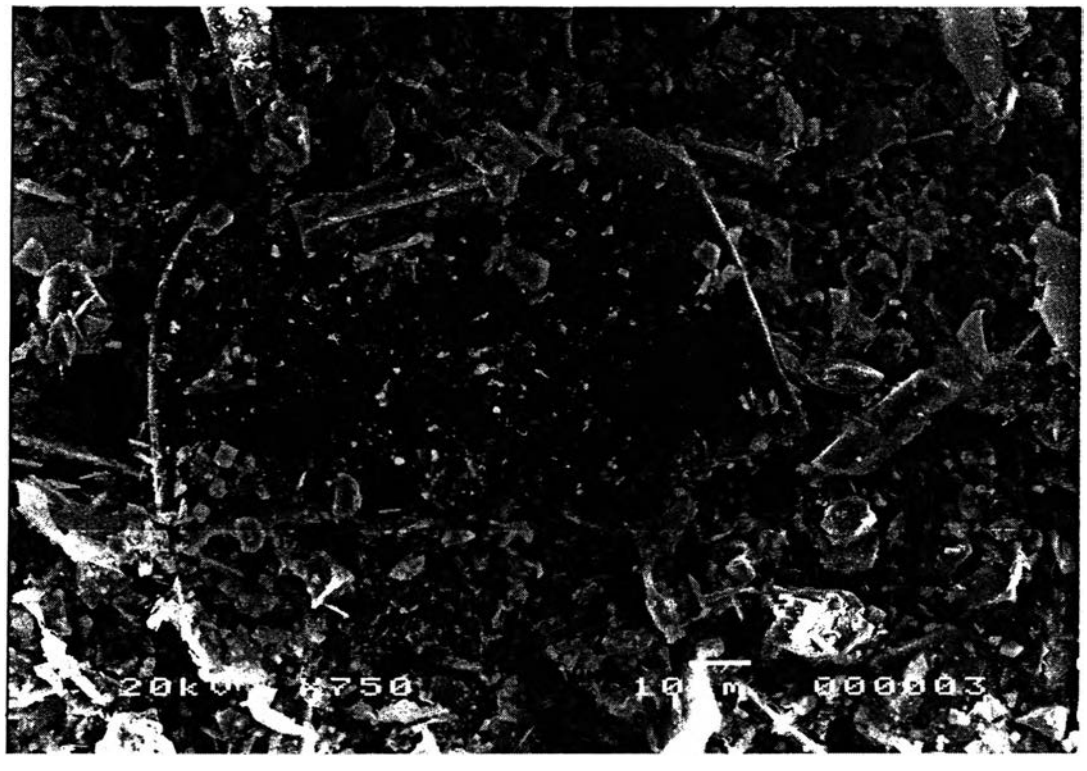

Figure 3.17 SEM of spinel powder prepared by sintering precursor obtained from the reaction of alumatrane and $Mg(OMe)_2$ at 1100°C for 2 h in air.